

# Lab on a Chip

Accepted Manuscript



This is an *Accepted Manuscript*, which has been through the Royal Society of Chemistry peer review process and has been accepted for publication.

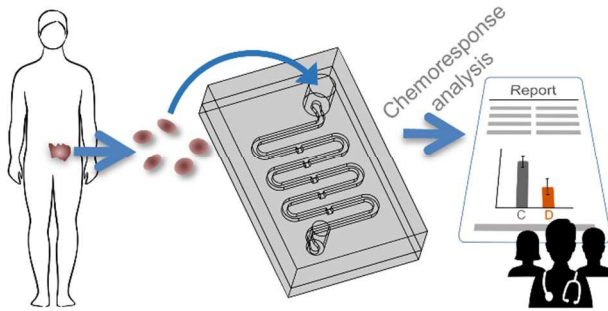
*Accepted Manuscripts* are published online shortly after acceptance, before technical editing, formatting and proof reading. Using this free service, authors can make their results available to the community, in citable form, before we publish the edited article. We will replace this *Accepted Manuscript* with the edited and formatted *Advance Article* as soon as it is available.

You can find more information about *Accepted Manuscripts* in the [Information for Authors](#).

Please note that technical editing may introduce minor changes to the text and/or graphics, which may alter content. The journal's standard [Terms & Conditions](#) and the [Ethical guidelines](#) still apply. In no event shall the Royal Society of Chemistry be held responsible for any errors or omissions in this *Accepted Manuscript* or any consequences arising from the use of any information it contains.

**Table of contents entry****20-word sentence describing the novelty of the work:**

Micro-dissected tumor tissues (MDTs) are maintained alive on chip for several days and show promising results for personalized medicine applications.

**Graphics (8 cm by 4 cm):**



## Lab on a Chip

## ARTICLE

## Micro-dissected tumor tissues on chip: an *ex vivo* method for drug testing and personalized therapy

Received 16th September 2015,  
Accepted xxth November 2015

DOI: 10.1039/x0xx00000x

[www.rsc.org/](http://www.rsc.org/)

M. Astolfi,<sup>b,c</sup> B. Péant,<sup>c</sup> M. A. Lateef,<sup>c</sup> N. Rousset,<sup>a</sup> J. Kendall-Dupont,<sup>c</sup> E. Carmona,<sup>c</sup> F. Monet,<sup>a</sup>  
F. Saad,<sup>c,d</sup> D. Provencher,<sup>c,e</sup> A.-M. Mes-Masson<sup>c,f</sup> and T. Gervais<sup>\*a,b,c</sup>

In cancer research and personalized medicine, new tissue culture models are needed to better predict the response of patients to therapies. With a concern for the small volume of tissue typically obtained through a biopsy, we describe a method to reproducibly section live tumor tissue to submillimeter sizes. These micro-dissected tissues (MDTs) share with spheroids the advantages of being easily manipulated on-chip and kept alive for periods extending over one week, while being biologically relevant for numerous assays. At dimensions below ~420 μm in diameter, as suggested by a simple metabolite transport model and confirmed experimentally, continuous perfusion is not required to keep samples alive, considerably simplifying the technical challenges. For the long term culture of MDTs, we describe a simple microfluidic platform that can reliably trap samples in a low shear stress environment. We report the analysis of MDT viability for eight different types of tissues (four mouse xenografts derived from human cancer cell lines, three from ovarian and prostate cancer patients, and one from a patient with benign prostatic hyperplasia) analyzed by both confocal microscopy and flow cytometry over an 8-day incubation period. Finally, we provide a proof of principle for chemosensitivity testing of human tissue from a cancer patient performed using the described MDT chip method. This technology has the potential to improve treatment success rates by identifying potential responders earlier during the course of treatment and providing opportunities for direct drug testing on patient tissues in early drug development stages.

### Introduction

Oncology drugs have a very low success rate in clinical trials and less than 7% of the drugs that proceed through all three trial phases are ultimately approved by the Food and Drug Administration (FDA), according to a recent United States based survey conducted between 2003 and 2011.<sup>1</sup> This low performance points to potential weaknesses in the current drug development pipeline. One obstacle may be that currently used preclinical models fail to correctly predict clinical outcomes in patients.<sup>2</sup> In addition, with a growing awareness that treatment response can be highly context dependent, there is a lack of proper patient stratification to prospectively identify subgroups of patients that will most likely benefit from new treatments.<sup>3</sup> Therefore, generating

more relevant models that could be used for preclinical testing or as a patient-specific drug-testing tool to guide the choice of a therapy would be of great interest to the cancer research community.

There is growing evidence that tissue tridimensionality, cellular composition, and micro-environment play an important role in cancer development and response to therapy. For these reasons, researchers need more sophisticated tissue based culture models in order to mimic critical features not represented in the traditional monolayer cultures.<sup>4-6</sup> Even animal models, mainly genetically modified mice and cancer cell line xenografts grown in immunodeficient mice, have limitations related to inherent biological features<sup>3</sup> as well as cost and time considerations. The field of tissue engineering strives to create new 3D models that reconstruct some of the important characteristics found in physiological tissues, but matching the complexity of *in vivo* tissues remains an important challenge.

Recent attention has focused on the use of spheroids that provide 3D models that begin to bridge the gap between monolayer cultures and tissues, as evidenced by several parameters including gene expression studies.<sup>7</sup> Spheroids can be reproducibly mass-produced from a number of established cell lines, although not all cell lines have the potential to form spheroids.<sup>8</sup> Due to their small size, they are compatible with microfluidic approaches and there are an increasing number of miniaturized devices specifically designed to study spheroids.<sup>9-</sup>

<sup>a</sup> Department of Engineering Physics, Polytechnique Montréal, Montreal, QC, Canada.

E-mail: thomas.gervais@polymtl.ca; Tel: +1-514-340-4711, ext. 3752.

<sup>b</sup> Institute of Biomedical Engineering, Polytechnique Montréal, Montreal, QC, Canada.

<sup>c</sup> Institut du cancer de Montréal and Centre de recherche du Centre hospitalier de l'Université de Montréal (CRCHUM), Montreal, QC, Canada.

<sup>d</sup> Department of Surgery, Faculty of Medicine, Université de Montréal, Montreal, QC, Canada.

<sup>e</sup> Division of Gynecologic Oncology, Faculty of Medicine, Université de Montréal, Montreal, QC, Canada.

<sup>f</sup> Department of Medicine, Faculty of Medicine, Université de Montréal, Montreal, QC, Canada.

† Electronic Supplementary Information (ESI) available. See DOI: 10.1039/x0xx00000x

<sup>13</sup> However, spheroids have a limited ability to mimic the complex tissue architecture and cell composition of human tumors and they do not reproduce the unique characteristics of specific patients' cancers. At their present level of development, spheroids provide limited advantages in the growing field of personalized medicine.

Employing patient-derived organotypic *ex vivo* cultures may provide a better model for the empirical testing of therapeutics. However, this approach has presented some significant hurdles, including the maintenance of viability over a sufficient number of days for different analytical purposes. In the absence of a functional vasculature, *ex vivo* primary tissues die prematurely, leaving little or no time to test a therapy and obtain a relevant readout. One approach has been to cut the tissue into thin (250-500  $\mu\text{m}$ ) slices of relatively large ( $\sim 4$  mm) diameter,<sup>14,15</sup> with the smaller dimension facilitating the transport of nutrients to the center of the tissue. Such samples have been cultured in microfluidic devices under continuous perfusion,<sup>16,17</sup> but their large format makes them challenging to process in microsystems and the cumbersome fluidic connections to a perfusion system reduce the number of independent tissue samples that can be assayed in parallel. To circumvent these problems, we propose a new tissue culture method combining the high biological relevance of patient-derived tumor slices with the manipulation simplicity in

microsystems of small spheroid-sized tissue samples. This novel tissue culture method can potentially be applied throughout the drug life cycle from preclinical testing to clinical patient response prediction guiding the selection of an optimal treatment regimen.

Conceptually, our proposed approach to enable treatment response assays on patient tissue (Fig. 1) first involves cutting limited amounts of a patient tumor, obtained through surgery or biopsy, into individual submillimeter-sized tissue sections. These micro-dissected tumor/tissue samples (MDTs) are then loaded into a specialized microfluidic platform in which small volumes of one or several drug candidates are tested directly on patient tissue in independent channels. The chemoresponse of the tissue is then evaluated and compared to non-treated controls in order to generate drug-response data specific to each patient.

To begin to address the challenges of this approach, we first derived theoretical evidence that sectioning tissue to submillimeter dimensions helps to maintain viability *ex vivo* by ensuring adequate oxygenation throughout the tissue, even without continuous perfusion. Based in part on 3D numerical simulations, we designed and created a simple microfluidic platform to trap and culture MDTs while shielding them from excessive shear stress. After refining the methodology to generate spheroid-sized MDTs, we experimentally validated

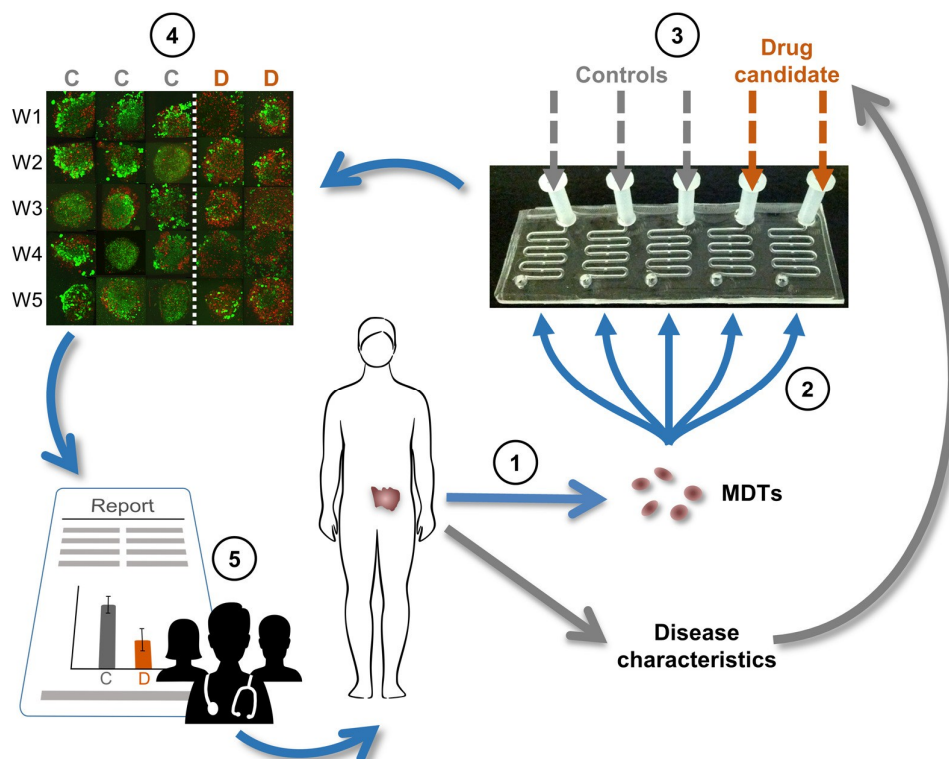


**Fig. 1:** Proposed approach to treatment selection using micro-dissected tumors on chip. 1) Tumor tissue is extracted from the patient, either through surgery or biopsy, and cut to multiple individual micro-dissected tumor samples (MDTs). 2) The MDTs are then loaded, trapped, and incubated within a microfluidic device composed of several channels, each able to trap five MDTs. 3) One or several selected drug candidates to be assessed are applied to MDTs in independent channels while other MDTs are kept as a non-treated controls. 4) After incubation with the drugs, the MDTs are analyzed by detecting live and dead cells using confocal microscopy or by measuring other drug-response parameters, and the results are compared to those of the non-treated controls. 5) Results are then interpreted to identify non responders to treatment and obtain useful information to elaborate a personalized treatment strategy.

that tissue viability is preserved within our microsystem for at least eight days without perfusion, with regular medium replacement, using MDTs produced from different types of tissues: xenografts derived from four different human cancer cell lines and four *ex vivo* tissues from patients. Finally, a proof-of-principle assay was performed using ovarian cancer tissue obtained from a patient to demonstrate that the procedure can generate patient-specific drug response data of potentially high clinical value.

## Theory

### Analysis of critical tissue size to avoid anoxia

Our goal is to prepare tissue sections that are large enough to mimic naturally occurring gradients of nutrients, waste and signaling molecules while also being small enough to maintain high viability throughout the tissue without risking anoxia in the center. As a non-polar molecule, oxygen ( $O_2$ ) dissolves only to low concentrations in medium (Table 1), which explains in part why most groups have chosen to continuously perfuse their tissue samples.<sup>16–19</sup> However, polydimethylsiloxane (PDMS) is a gas-permeable polymer that is often used to fabricate microsystems. As demonstrated experimentally using spheroids,<sup>20</sup> if the tissue samples are sufficiently small, it becomes possible to maintain adequate levels of  $O_2$  in non-perfused medium by taking advantage of the PDMS material property.

In a seminal paper on anoxia in human tumors, Thomlinson and Gray<sup>21</sup> used a simple  $O_2$  consumption model to explain the formation of necrotic cores in cylindrical non-vascularized human lung tumors and to obtain a critical tissue thickness above which anoxia is induced. Others have contributed to the development of models to characterize the distribution of nutrients and waste in spherical samples,<sup>22–26</sup> especially to study spheroids. In order to justify the pertinence of dissecting the tumor samples to submillimeter sizes and to determine optimal dimensions to avoid complete depletion of  $O_2$  in the center of MDTs, we derived a simple diffusion-reaction model of  $O_2$  consumption for non-vascularized spherical tissue samples. Our model supposes that  $O_2$  is consumed at a constant rate (zero-order reaction kinetics), following previous studies,<sup>21–23,26</sup> despite knowing that cells can modulate their consumption as a function of the available  $O_2$  concentration.<sup>24,27,28</sup> This simple approach guarantees a lower

bound on the maximum tissue diameter before  $O_2$  is depleted. Indeed, all other reaction kinetics models of higher order (1<sup>st</sup> order, Michaelis-Menten, etc.) would set reduced consumption rates in the presence of lower  $O_2$  concentrations and consequently derive a higher critical diameter before hypoxia sets in.

In non-perfused conditions, the distribution of  $O_2$  inside and around the tissue follows a diffusive process. Within the tissue,  $O_2$  is additionally consumed by the cells. The equation describing these mass transfer phenomena is:

$$\frac{\partial C}{\partial t} = D\nabla^2 C - q, \quad (1)$$

where  $C$  is the concentration of  $O_2$ ,  $t$  is the time,  $D$  is the diffusion constant of  $O_2$  and  $q$  is the volumetric  $O_2$  consumption rate. The 3D space is partitioned into two subdomains of live tissue and medium surrounding it, with a continuity boundary condition linking both of them. The analysis was further simplified by placing the MDT in an infinite aqueous medium rather than in a PDMS device, and assuming spherical symmetry. We also exclude the necrotic core subdomain as it is unnecessary for the purpose of the demonstration outlined here. All these simplifications again yield a lower boundary on the critical diameter because  $O_2$  in PDMS has both a greater permeability and diffusivity than in water (ESI Table S1). The other boundary conditions are zero concentration at the center of the tissue ( $C(r = 0) = 0$ ) and maximum dissolution concentration of  $O_2$  in medium at infinity ( $C(r \rightarrow \infty) = C_{max}$ ). Outside the tissue, the  $O_2$  consumption term  $q$  falls to zero. Assuming steady state ( $\partial C / \partial t = 0$ ) and solving the subdomain differential equations for radius  $r$ , the following expression of the non-perfused critical diameter ( $2R_C$ ) is found (see ESI for details):

$$2R_C = 2 \sqrt{\frac{6D_T D_M C_{max}}{\rho Q (2D_T + D_M)}}. \quad (2)$$

The critical diameter depends on the diffusivity constant of  $O_2$  in the tissue ( $D_T$ ) and in the medium ( $D_M$ ), on the maximum dissolution concentration of  $O_2$  in aqueous medium ( $C_{max}$ ), and on the volumetric  $O_2$  consumption rate by the tissue ( $q = \rho Q$ ) where  $\rho$  is the tissue density and  $Q$  is a constant  $O_2$  consumption rate per unit mass of tissue.

**Table 1:** Description of the variables for the calculation of oxygen ( $O_2$ ) concentration in a tissue sample and in the surrounding medium

Variable	Description	Value	References
$C_{max}$	Maximum dissolution concentration of $O_2$ in water at 37°C and at 0.2 atm (partial pressure of $O_2$ in a cell incubator)	0.20 mol/m <sup>3</sup>	Henry's Law; Sander <sup>29</sup>
$Q = q/\rho$	Maximum $O_2$ uptake rate per cell	$7.37 \times 10^{-17}$ mol/s	Average from literature <sup>30–34</sup>
$\rho$	Density of cells in cancerous tissue	$2.76 \times 10^{14}$ cells/m <sup>3</sup>	Experimental value
$D_T$	$O_2$ diffusivity constant in cancerous tissue at 37°C	$1.83 \times 10^{-9}$ m <sup>2</sup> /s	Average from literature <sup>23,33–36</sup>
$D_M$	$O_2$ diffusivity constant in water at 37°C	$2.62 \times 10^{-9}$ m <sup>2</sup> /s	Han & Bartels <sup>37</sup>
$q$	Maximum $O_2$ uptake rate per volume of tissue	Calculated ( $Q \times \rho$ )	N/A
$R_C$	Critical radius of a non-perfused spherical tissue section	Calculated (equation 2)	N/A
$R_{CP}$	Critical radius of a perfused spherical tissue section	Calculated (equation 3)	N/A

Using parameters found in the literature<sup>28,29,36,37</sup> or measured experimentally for tumor tissue and aqueous solutions (Table 1), a critical diameter equal to 424  $\mu\text{m}$  was calculated according to equation (2). By keeping all dimensions of a tissue sample below this critical point, perfusion thus becomes unnecessary to maintain sufficient  $\text{O}_2$  levels.

Under continuous perfusion, fresh oxygenated medium is constantly supplied by convection at the surface of the tissue. In mass transport terms, the effect of perfusion is equivalent to an increase of the apparent diffusion constant of  $\text{O}_2$  in the medium. In the extreme case of infinitely fast perfusion around the tissue, mass transfer occurs across an infinitely thin boundary layer, which is equivalent in our model to setting medium diffusion constant to infinity ( $D_M \rightarrow \infty$ ). Setting this condition in equation (2) yields an expression for the critical diameter ( $2R_{\text{CP}}$ ) in perfectly perfused conditions:

$$2R_{\text{CP}} = 2 \sqrt{\frac{6D_T C_{\text{max}}}{\rho Q}}. \quad (3)$$

Thus, we conclude that perfusion would only increase the critical diameter slightly, i.e. by a factor up to  $\sim\sqrt{3}$  in the current example.

These simple calculations that only take  $\text{O}_2$  into account were used as a guideline to select optimal MDT size in our experimental setup. According to these calculations, perfusion could be avoided altogether without any risk of anoxia if MDTs have diameters of  $d < 424 \mu\text{m}$ . Other nutrients such as glucose are also essential to the metabolic activity of tissue sections. To complete the analysis, the consumption of oxygen and glucose in the PDMS microsystems was therefore studied using 3D numerical simulations (see Results section).

## Materials and methods

### Fabrication of a microfluidic incubation device for MDTs

Each microfluidic platform is composed of two PDMS replicas obtained from micromachined master molds. The bottom PDMS layer forms five open channels with a 600  $\mu\text{m}$ -wide square cross-section, each containing five 600  $\mu\text{m}$ -wide square-bottom microfluidic wells of 500  $\mu\text{m}$  in height. The top layer is composed of 3 mm diameter inlet holes and 2 mm diameter outlet holes, and closes the upper side of the channels once assembled with the bottom layer (ESI Fig. S1). The molds were carved out of poly(methyl methacrylate) blocks using 3.57 mm and 1 mm diameter end mills controlled by a computerized numerical control machine. Liquid PDMS (Sylgard® 184 silicone elastomer kit, Dow Corning, Midland, USA) prepared at a base polymer to curing agent mass ratio of 10:1 was poured into each mold, degassed, and cooked at 80°C for 1.5 hours. The platform was assembled by plasma-bonding the two PDMS layers together and by fitting hollow nylon cylinders (#91145A138, McMaster-Carr, Elmhurst, USA) into the inlet holes of the top layer to form a larger inlet reservoir (ESI Fig. S1).

### Production of human prostate and ovarian cancer xenografts in mice

Four different human carcinoma cell lines derived from prostate cancer tumors (22Rv1 and PC3, ATCC, Manassas, USA) and ovarian cancer tumors (TOV112D) or ascites (OV90)<sup>38</sup> were used to produce mouse xenografts. Cell suspensions were obtained after amplification in 2D cultures and mixed with Matrigel® (BD Biosciences, Franklin Lakes, USA) before being subcutaneously injected into severely combined immunodeficient NOD SCID male mice (Charles River Development, Burlington, USA) for 22Rv1 and PC3, or female mice for TOV112D and OV90 cells lines. Solid tumors were formed and harvested after growth periods varying from 21 to 70 days depending on the cell line injected. All protocols involving animals were reviewed and approved by the Comité institutionnel de protection des animaux (CIPA) at the CRCHUM.

### Patient tissues

Patient tissue specimens were collected from patients following informed consent from the Centre hospitalier de l'Université de Montréal (CHUM), Division of Gynecologic Oncology and the Uro-Oncology Service. They were kept on ice until the sectioning procedure was initiated within three hours. This part of the study involving human samples was approved by both institutional ethics committees: the Comité d'éthique de la recherche du CHUM (CÉR-CHUM) and the Comité d'éthique de la recherche de l'École Polytechnique de Montréal.

### Tissue sectioning procedure

To produce the MDTs, thin tumor tissue fragments (~1 mm by 5 mm) were cut using a scalpel and embedded into 3.7% low melting point (LMP) agarose (Thermo Fisher Scientific, Waltham, USA) supplemented with 10% fetal bovine serum (FBS, BD Biosciences), kept liquid at 40-45°C. The agarose was solidified on ice for at least 30 minutes, thereby creating a supporting structure around the embedded tissue. A traditional vibratome (The Vibratome Company, St. Louis, USA) was used to produce 300  $\mu\text{m}$ -thick tissue slices, inside a 15°C bath containing Hank's Buffered Saline Solution (HBSS, #311-516-CL, Wisent Inc., Saint-Bruno-de-Montarville, Canada) supplemented with 10% FBS, 55 mg/L gentamicin (Wisent Inc.), and 600  $\mu\text{g}/\text{L}$  amphotericin B (Wisent Inc.). The produced slices were kept in the same solution and finally further cut into disk-like MDTs using a 500  $\mu\text{m}$  diameter tissue punch (Zivic Instruments, Pittsburgh, USA). The final product was a cylindrical MDT of approximately 300  $\mu\text{m}$  in height and 380  $\mu\text{m}$  in diameter.

### Device operation for culturing MDTs

The microfluidic systems were first treated overnight with a 10 mg/mL solution of triblock copolymer (Pluronic® F-108, Sigma-Aldrich, St. Louis, USA) in order to reduce cell adhesion to the PDMS surfaces.<sup>39</sup> Air bubbles were then removed from

the channels using 100% ethanol, and the devices were sterilized by applying 70% ethanol for 15 minutes. The channels were thoroughly rinsed with non-supplemented sterile HBSS and placed in a humidified cell incubator (37°C, 5% CO<sub>2</sub>, 95% ambient air).

Once the MDTs were produced, the devices were removed from the incubator and placed under a stereoscope for the MDT loading procedure. With the inlet filled with HBSS, five MDTs were collected using a 20 µL micropipette and allowed to sediment to the bottom of the inlet inside the microreservoir. Flow was induced within the channel by aspirating liquid from the outlet using a micropipette and MDTs were carried inside the channels with the flow. By either aspirating or ejecting liquid from the outlet, the MDTs were steered within the channel. Flow was stopped for 1-2 seconds when an MDT was positioned above an empty well, allowing it to sediment to the bottom. Once all five MDTs loaded, the loading medium was rinsed two times by adding culture medium to the channels: either OSE (#316-031-CL, Wisent Inc.) for ovarian cancer or RPMI 1640 (# 350-045-CL, Wisent Inc.) for prostate cancer MDTs, both supplemented with 10% FBS, gentamicin and amphotericin B and warmed to 37°C. With about 20 µL of medium left in the inlet, the loaded devices were kept within a perforated and humidified box, inside the cell incubator.

One, three, six, and eight days following MDT production, medium was replaced in each system. All collected media was kept at 4°C for further analysis in flow cytometry experiments.

#### Chemotherapy treatment of patient-derived MDTs

One set of patient MDTs was used to test the chemosensitivity of the tissue to standard treatment. Since the tissue was provided from a patient with high-grade serous ovarian cancer, carboplatin (Hospira, Lake Forest, IL USA) at a concentration of 350 µM was applied directly within the device. Treatment was initiated one day following the surgery, renewed after one day of incubation, and removed one day later (i.e. three days after surgery). Two independent channels were treated with carboplatin and three were kept as non-treated controls.

#### On-chip live-tissue imaging by confocal microscopy and image processing

Confocal microscopy was employed as an endpoint assay to measure the viability of samples. Multiple systems were thus analyzed at different time points to reflect the evolution of cell viability over the whole 8-day incubation period. Dual fluorescent staining of the MDTs was performed at different time points using CellTracker™ Green CMFDA (CTG, Thermo Fisher Scientific) labelling viable cells and propidium iodide (PI, Sigma-Aldrich) labelling the nucleic acids of dead cells. Solutions of HBSS containing either CTG (5 µM) alone or a combination of both CTG (5 µM) and PI (1.5 µM) were added to the systems sequentially by following the medium replacement procedure. MDTs were first incubated one hour with the CTG solution, and then an additional 30 minutes with

both dyes. After replacing the dye solutions with HBSS, the samples were imaged.

To minimize autofluorescence, the upper thresholds for the microscope settings (laser power and detector gains) were determined by first imaging non-labelled MDTs incubated under the same conditions within the microfluidic system and ensuring minimal signal detection. The platforms were held with a microscope slide holder over the 20X dry objective of an inverted Leica TCS SP5 II confocal microscope (Leica Microsystems, Wetzlar, Germany). The labelled MDTs were then imaged directly through the thin PDMS layer underneath the platform in 10 µm-spaced optical slices. CTG and PI were independently excited with the 488 and 561 nm laser lines and their fluorescence signal was collected in the wavelength ranges 500-550 nm and 600-700 nm, respectively. Maximum projections, which are 2D representations of the 3D z-stack acquisitions, were computed for each MDT.

A custom-built MATLAB (MathWorks, Natick, USA) algorithm was used to analyze each focal image of the acquired MDT z-stacks based on the ratio of the area occupied by CTG-labelled cells over the total area of both CTG- and PI-labelled cells (see details in ESI). The reported MDT diameters were calculated from confocal microscopy projection images as the average of two perpendicular (horizontal and vertical) diameter measurements per MDT.

#### Off-chip analysis of dissociated cells by flow cytometry

Fluorescence-activated cell sorting (FACS) was also used as an end-point assay to measure the survival of individual cells constituting the MDTs after their incubation in the platform. The MDTs were first labelled within the microsystems using the apoptotic fluorescent dyes annexin V (3:100 dilution) and 7AAD (5:100 dilution) (PE Annexin V Apoptosis Detection Kit I, BD Biosciences). The relatively high surface roughness of our PDMS replicas lead to reduced plasma bonding strength, which was exploited to extract MDTs from the microsystems for off-chip analysis. Sharp scissors were used to initiate the separation of the two PDMS layers which were then peeled apart without affecting the position of MDTs in their sedimentation traps. All five MDTs from a single system were individually pipetted out of their wells and pooled in the same tube for analysis, together with all the medium fractions collected at previous time points which were also labeled thus ensuring that all cells were analyzed. The five MDTs from a single channel were dissociated into single cells by incubating them for 15 minutes at 37°C in 400 µL of a saline solution supplemented with 0.25 mg/mL collagenase IV (#LS004209, Worthington Biochemical Corp., Lakewood, USA). Samples were rinsed twice and reconstituted in 500 µL of buffer. Prior to the analysis by the flow cytometer (LSR-Fortessa, BD Biosciences), cell suspensions were passed through a 35 µm cell strainer (#352235, Corning Inc., Corning, USA). Some MDTs were submitted to the same treatment, but without the staining step. They were used, together with positive controls, to set the PMT levels and thresholds in the annexin V and 7AAD fluorescent channels. The data from each acquisition

was analyzed using FlowJo (FlowJo LLC, Ashland, USA) by gating the cell population in the front scatter/side scatter (FSC/SSC) graph, removing doublets, and associating each cell to one of three populations according to its fluorescent labelling: early apoptotic cells (annexin V-stained only), late apoptotic or dead cells (double stained with annexin V and 7AAD), and live cells (non-stained).

#### Culture of large tissue fragments

For comparison, xenograft tissue was also cut to larger sections of approximately 8 mm<sup>3</sup>, named large tissue fragments (LTFs). Nine to ten LTFs were cultured in a 60 mm Petri dish (#83.3901, Sarstedt, Nümbrecht, Germany) in 12 mL of the same medium as the one used for MDTs (as defined above). After 30 minutes of incubation, medium was changed and samples were kept in a cell incubator (37°C, 5% CO<sub>2</sub>). Medium was changed at the same intervals as for MDTs. At specific time points, each LTF (or a group of five MDTs) was dissociated into single cells by incubating it for 15 minutes at 37°C in 400 µL of a saline solution supplemented with 1 mg/mL of collagenase crude (#C9407, Sigma-Aldrich) and 0.25 mg/mL of collagenase type 1A (#C9891, Sigma-Aldrich). The cell suspensions were then rinsed twice, reconstituted in 100 µL of binding buffer, and stained with the apoptotic fluorescent dyes annexin V (3 µL) and 7AAD (5 µL) (PE Annexin V Apoptosis Detection Kit I, BD Biosciences). Volumes were finally brought up to 500 µL before the samples were analyzed by flow cytometry, as detailed above. MDTs used for this comparison were prepared for FACS analysis under the same conditions as described in this section for LTFs.

#### Device characterization with 3D numerical simulations

The finite element method with the commercial COMSOL Multiphysics® software was used to model the device and simulate both convective flow and diffusion. The device model was drawn to scale using the built-in COMSOL geometry drawing tools. The parameters applied to the models can be found in the ESI Table S1. Convective flow was defined using the Navier-Stokes equations for incompressible flow while diffusion was defined using the reaction-diffusion equation with Michaelis-Menten kinetics. These convection and diffusion differential equations were solved using, respectively, the built-in steady-state fully coupled solver for laminar flow and the built-in transient segregated solver. A user-defined mesh was necessary to reach a sufficiently accurate result of flow and diffusion around smaller MDTs. A parametric sweep of inlet flow and MDT dimensions was done to fully characterize operating conditions of the device. Maximum shear stress on the MDT, lift forces on the MDT and minimum metabolite concentration in the MDT were probed for each solved parameter with the built-in component coupling functions.

## Results

### Microfluidic device design

**Channel configuration.** Each 100% PDMS platform is made up of two fluidic levels: the top level where the samples circulate through channels to their traps and the bottom level composed of square-bottom wells where the samples sediment (Fig. 2A-C). Five independent channels fit on a 2.5 cm by 7.5 cm surface (equivalent to that of a standard glass slide), making it possible to trap up to 25 individual MDTs and to submit them to five different treatment conditions. The distance between the traps ensures that each MDT has access to a maximum amount of nutrients in non-perfused conditions and the total channel volume of about 30 µL makes it possible to control the samples using a 20 µL micropipette. Each channel is laid out in a serpentine fashion and can be viewed entirely in the field of view of a low magnification stereoscope. The channel cross-section is 600 µm by 600 µm. The gravitational square-bottom traps are 600 µm in width by 500 µm in height. These dimensions have been tested to accommodate disk-like tissue samples with diameters of 381 ± 47 µm (mean ( $\mu$ ) ± standard deviation ( $\sigma$ ), Fig. 2H) by 300 µm in height.

**Loading of MDTs.** With average sphericities of 0.87, cylindrical MDTs of reproducible sizes were obtained by producing 300 µm-thick tissue slices using a vibratome and by further micro-dissecting the slices using a biopsy punch (Fig. 2D). Tissue diameter fluctuations could in part be due to variable tissue elasticity. For the MDTs to enter the channels, they were deposited at the bottom of the inlet, inside the microreservoir, and flow was induced by aspirating fluid from the outlet (Fig. 2E). Samples located in the microreservoir (Fig. 2E, inset) were submitted to a higher flow velocity than if they were positioned elsewhere in the inlet, which facilitated their entry into the microchannels. To trap the MDTs, flow was again induced in the desired direction. Under a stereoscope, a user observed the tissue samples circulating within the device and manually positioned them above their respective wells where they were trapped by sedimentation (Fig. 2E). This method was very effective at avoiding multiple MDTs getting trapped in the same well since the user precisely controlled the flow with the micropipette, accelerating, decelerating, or reversing it as needed. Complete loading of a channel with five samples, as shown in Fig. 2F, was generally accomplished in less than a minute (ESI Video S1).

**Gravitational trapping mechanism.** The MDTs, once positioned above a trap, are gravity-driven into the microfluidic square wells. Two conditions must be met for gravitational trapping to succeed: the MDT needs a positive differential density compared to the surrounding medium and the sedimentation time into the trap has to be shorter than the travelling time over the trap. The equation describing the steady-state velocity at which a sphere sediments in an infinite fluid compartment ( $v_{inf}$ ) is derived from Newton's second law

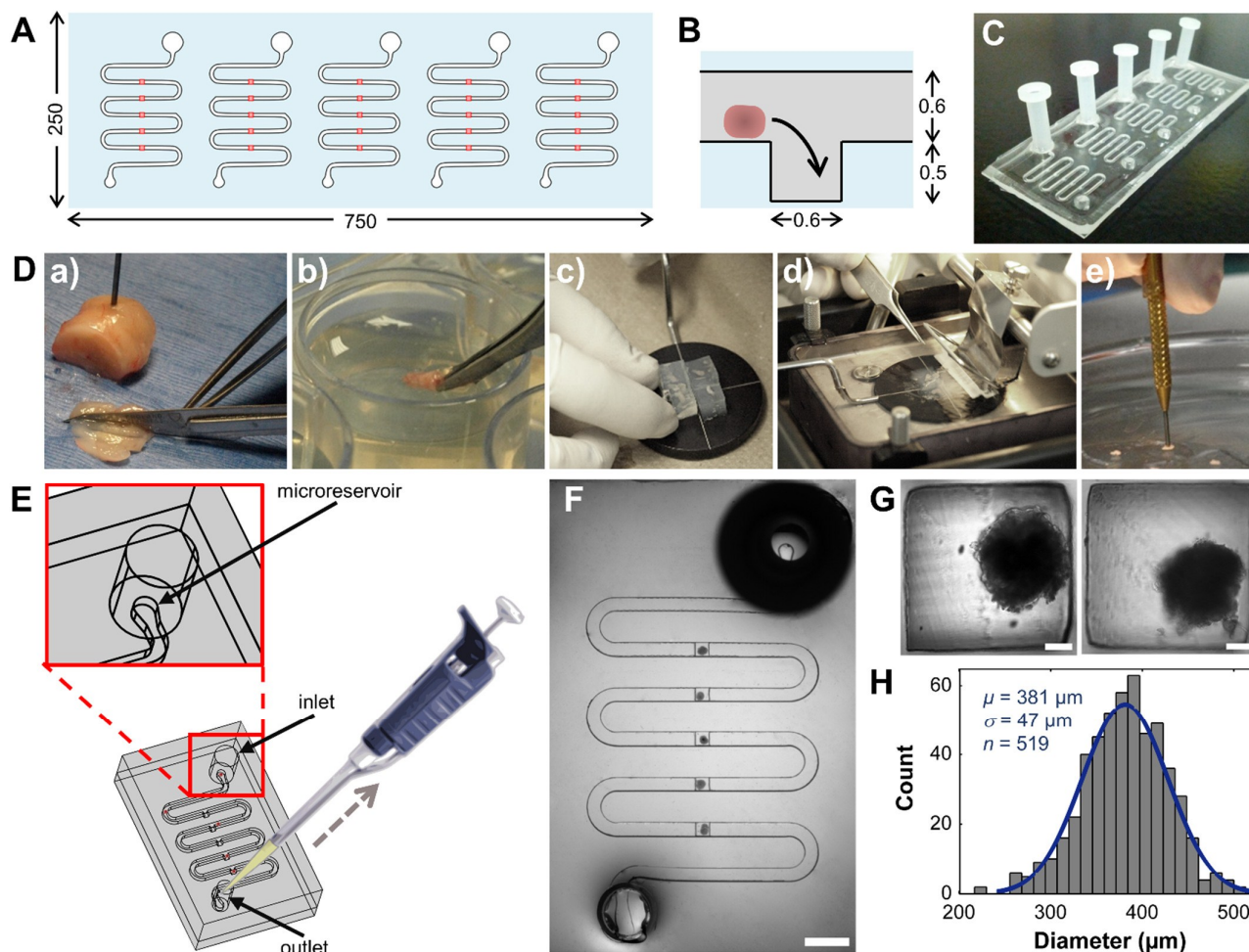


**Fig. 2:** Microfluidic device design and loading of MDTs. A) Top view of a microfluidic device showing five independent channels (black contours) of 78 mm in length, each containing five equally-spaced microfluidic traps (red); dimensions in mm. B) Side view schematic of a MDT in the loading channel near a sedimentation trap; dimensions in mm. C) Picture of an assembled device made of two PDMS layers and five inlet reservoirs. D) MDT micro-dissection technique: a scalpel is used to form thin tissue fragments (a) that are then embedded in a LMP agarose matrix (b and c), a vibratome is used to produce 300  $\mu\text{m}$ -thick slices (d), and the tissue slices are further cut into disk-like samples using a 500  $\mu\text{m}$  biopsy punch (e). E) Procedure to load MDTs into the channel using a micropipette to induce fluid flow and position MDTs above traps where they sediment. F) Top-view picture of a microfluidic device loaded with a MDT in each of the five square traps; scale bar: 2 mm. G) Close-up view of traps loaded with MDTs; scale bars: 100  $\mu\text{m}$ . H) Diameter distribution of 519 MDTs; average:  $\mu = 381 \mu\text{m}$ , standard deviation:  $\sigma = 47 \mu\text{m}$ .

by considering the drag force opposed to the gravity force exerted on a sphere:<sup>40</sup>

$$v_{\text{inf}} = \frac{\Delta\rho g d^2}{18\eta}, \quad (4)$$

where  $\Delta\rho$  is the particle to medium differential density,  $g$  is the gravitational acceleration,  $d$  is the particle diameter, and  $\eta$  is the fluid viscosity. The differential density ( $\Delta\rho$ ) of MDTs of known sizes was determined experimentally with equation (4) by timing MDT sedimentation in a large tube with diameter  $d_{\text{tube}} \gg d$ . An average experimental relative density of  $21 \pm 6 \text{ kg/m}^3$  was found (ESI Table S2). Larger spheres of same density sediment more rapidly ( $v_{\text{sed}} \propto d^2$ ), which explains why tissue samples ( $d \sim 380 \mu\text{m}$ ) would settle about 1500 times faster than single cells ( $d \sim 10 \mu\text{m}$ ) in an infinite compartment, making this trapping method more efficient for particles of larger diameter.

However, since the width ( $w$ ) of the microfluidic traps is comparable to the diameter of the MDTs, the walls significantly slow down the sedimentation process by adding a drag component to the movement of the particle.<sup>41–43</sup> This effectively reduces the sedimentation velocity of MDTs by a factor of 6 to 16 depending on MDT size based on our numerical simulations which consider a falling sphere in a bottomless long square trap (see figure 3A inset). This retardation factor ( $v_{\text{sed}}/v_{\text{inf}}$ ) can be precisely accounted for using a quadratic fit (Fig. 3A). Nonetheless, taking into account these wall effects and considering a trap of finite depth, MDTs sediment to the bottom of the wells – over a total distance of 500  $\mu\text{m}$  – in less than two seconds.

As shown in Fig. 3B, under a steady flow rate, MDTs are subjected to drag forces pinning them in the upstream portion of the well and exerting a lift force upon them. The magnitude and direction of the resulting force is a function of tumor, channel, and well dimensions.<sup>44</sup> Their position at the bottom

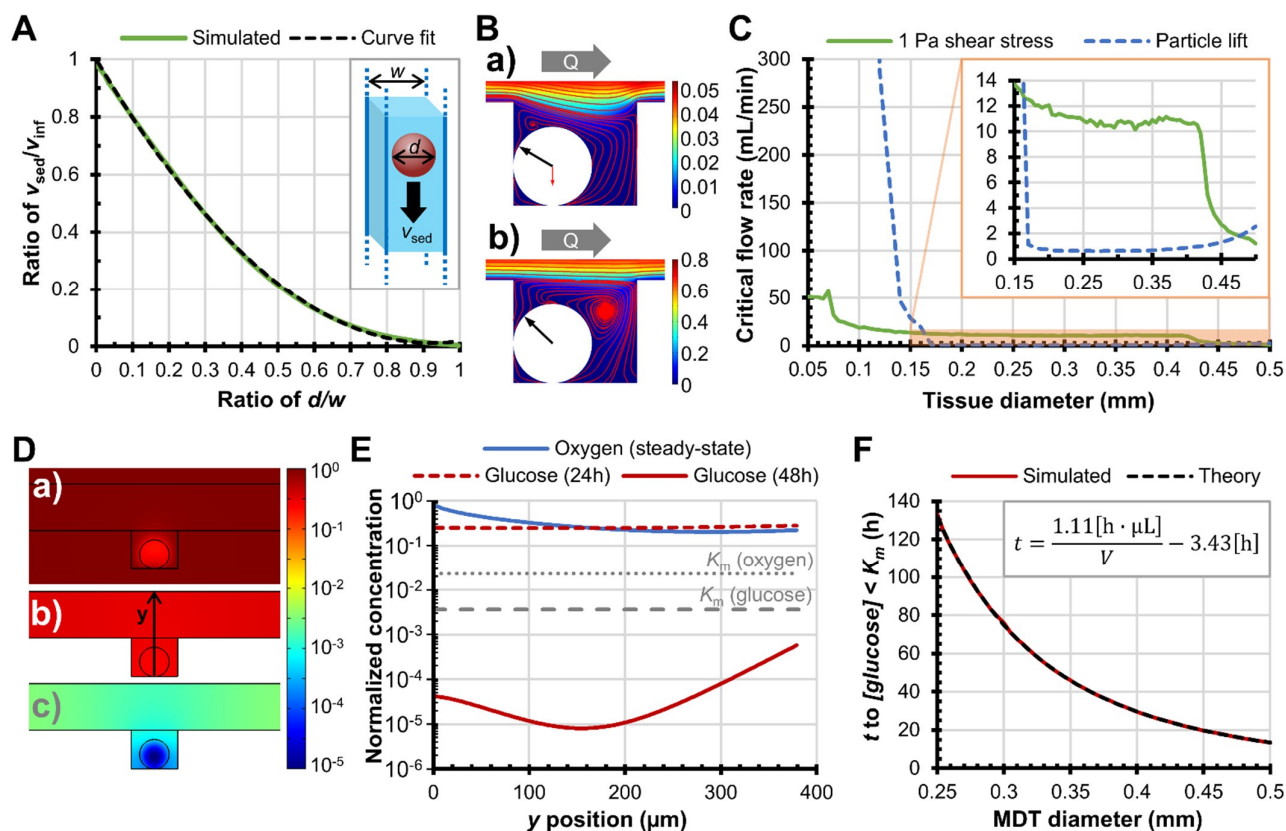


**Fig. 3:** Device characterization using 3D numerical simulations. A) Wall effect velocity correction ratios for MDTs of different dimensions sedimenting in square cross-section traps of infinite length (inset). Quadratic curve fit:  $v_{sed}/v_{inf} = 1.15(d/w)^2 - 2.13(d/w) + 1$ . B) Streamlines, gravitational force on MDTs (red arrow – negligible for (b)), hydrodynamic force on MDTs (black arrow) and fluid velocity colormap in  $m/s$  at flow rates ( $Q$ ) provoking particle lift (a) and inducing shear stress superior to 1 Pa (b). C) Critical flow rate leading to MDT ejection from the wells (blue dashed line) or inducing shear stress on MDT surface superior to 1 Pa (green solid line) for different MDT diameters. D) 3D simulations of  $O_2$  and glucose consumption by an average sized MDT ( $381 \mu m$ ) showing a cross-sectional view of the distribution of  $O_2$  at steady state (a), glucose after 24 h (b) and glucose after 48 h (c) through the system. E) Metabolite concentration along the  $y$ -axis (as defined in D) inside a trapped MDT of average size ( $381 \mu m$ ) normalized to initial  $O_2$  and glucose concentration in culture medium. Michaelis-Menten ( $K_m$ ) constants are shown for  $O_2$  (grey dotted line) and glucose (grey dashed line). F) Time ( $t$ ) before glucose concentration  $[glucose]$  falls below  $K_m$  for different MDT diameters.

of the wells is stable unless the net vertical hydrodynamic force (lift) on the MDT exceeds gravitational trapping, thus ejecting it from the well. In general, exceeding critical flow rates may lead to either ejection of the MDT or high shear stresses likely to cause cellular damage. Figure 3C shows that, for tissue sizes within our experimental distribution (Fig. 2H), MDTs are ejected from the trap before being subjected to high shear stresses. Relatively high flow rates are necessary to reach these critical values since flow penetration in the trap is minimal, causing the fluid velocity around the sample to remain under 10% of that in the channel.

#### Mass transport characterization in non-perfused conditions

Diffusion is the main transport mechanism *in vivo* between capillaries and the surrounding tissue. Similarly, within the microfluidic platform, diffusion between the channel and traps allows the tissue samples to access nutrients, drugs and other reagents provided through the medium, and to dispose of their cellular waste. When fresh medium is added through the channels, only the layers of fluid near the channel are renewed instantly whereas the solution within the traps mostly

recirculates. Gradually, nutrients from the channel diffuse into the traps and waste molecules diffuse out. Since diffusion times depend on the size of the molecules, small molecules such as ions diffuse rapidly in and out of the traps whereas larger molecules such as glucose take more time (~3.5 minutes).

Since the  $O_2$  saturation level in medium is low, an alternate influx of  $O_2$  is necessary to ensure that non-perfused samples have enough  $O_2$  for normal cell metabolism. In our case, the gas-permeable PDMS walls of the system provide this influx. In steady-state, our simulations show that  $O_2$  levels are ample within our microfluidic device to maintain samples viable (Fig. 3D-E).

However, other nutrients have no external influx and cellular waste accumulates through the system. Consequently, medium needs to be changed frequently in non-perfused conditions. Glucose, for example, is continuously consumed by the MDTs and may be depleted if the system is left unattended for too long. According to our simulations, we show that although glucose is abundant after 24 hours, its concentration falls below the Michaelis-Menten constant ( $K_m$ ) after 35 hours for average-sized MDTs (Fig. 3F). This  $K_m$  value indicates the

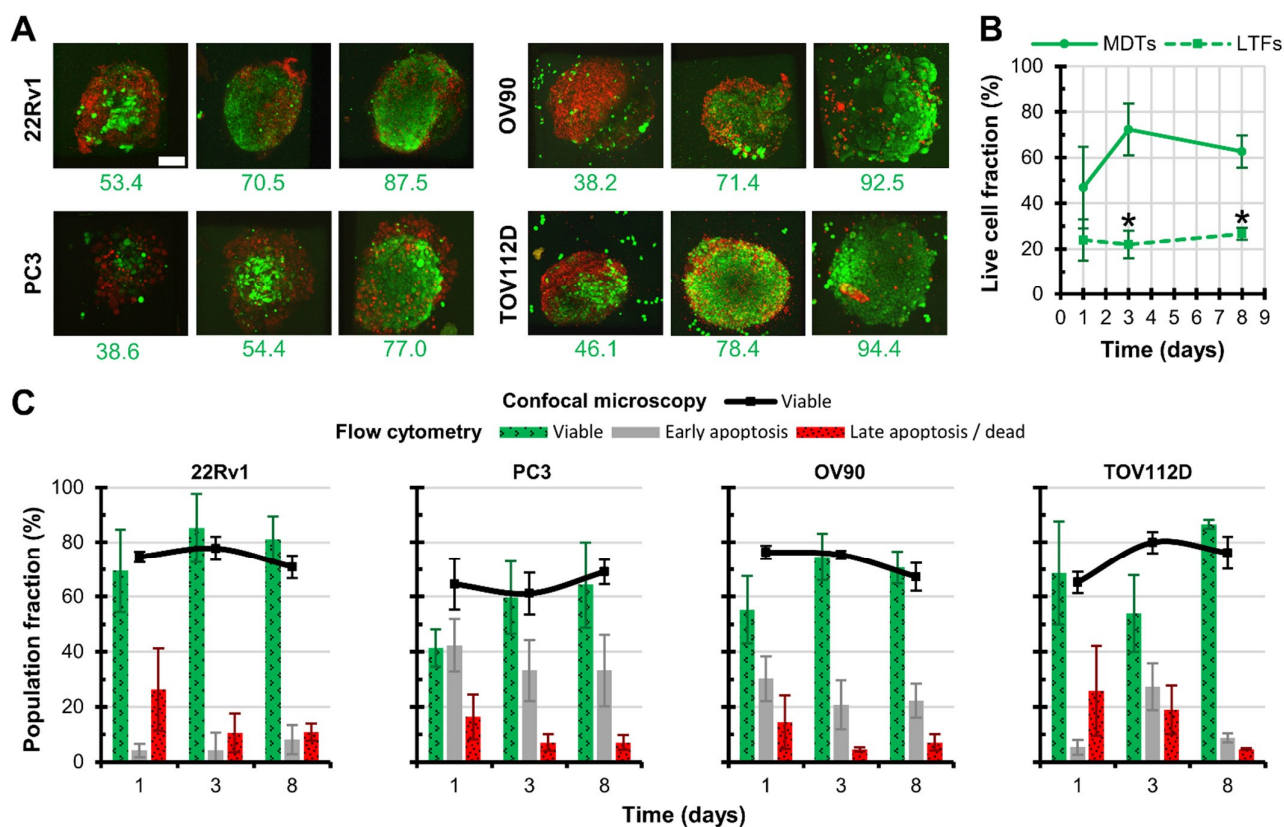


**Fig. 4:** Long-term viability of non-treated MDTs analyzed by confocal microscopy and by flow cytometry. A) Maximum projection images of confocal optical slices showing examples of MDTs labelled with viability dyes – CTG (live, green) and PI (dead, red) – and corresponding viability score calculated by the automatic image segmentation algorithm. B) Live cell fraction as a function of time, measured by FACS, for LTFs (dashed line) compared to MDTs (solid line) formed from different xenografts pooled in the same graph. Error bars: standard error of the mean for four independent experiments. \*p-value < 0.05 for the t-test comparing values for LTFs to those for MDTs. C) MDT survival over an 8-day incubation period for four types of xenografts, analyzed by confocal microscopy (black lines: viable) and by flow cytometry (bar graphs, green: viable, grey: early apoptosis, red: dead or late apoptosis). The results for an overall total of 427 MDTs from 26 xenografts are represented. Error bars: standard error of the mean for at least two independent experiments.

concentration at which the Michaelis-Menten uptake of a nutrient is reduced to half its maximum rate. As this rate keeps dropping due to the finite amount of glucose, cells slowly transition from proliferating to quiescent or dying states.<sup>45</sup> Since the cell-cycling process is slow (taking up to 1 day),<sup>46</sup> changing the medium at 2 to 3 days interval is necessary to avoid glucose deprivation possibly leading to cell death.

Figure 3F also shows that smaller MDTs take a longer time than larger ones to deplete a similar amount of glucose within the tissue. The inversely proportional scale between time to reach  $K_m$  and MDT volume can be derived by solving equation (1) for glucose transport (see ESI for details).

As shown in Fig. 3D-E, due to tissue tridimensionality, natural gradients of nutrients and waste exist within the MDTs from the outer surface to the center. The device asymmetry along the y axis from the bottom of the trap to the top of the channel causes a decentralization of the minimum nutrient concentration position within the tissue. This minimum is slightly displaced towards the bottom of the sample for glucose, since glucose comes from the channel. In contrast, it is displaced towards the top for  $O_2$ , since the diffusion constant of  $O_2$  through water is slightly inferior to that through

PDMS (ESI Table S1) and therefore, the more abundant source of  $O_2$  is from the bottom of the device.

#### Long term survival of non-treated xenograft derived MDTs

As a first step to demonstrate the effectiveness of our systems to trap and maintain live MDTs, we assessed the survival of non-treated MDTs obtained from four different types of mouse xenografts derived from two human prostate cancer (22Rv1 and PC3) and two human ovarian cancer (OV90 and TOV112D) cell lines. Over a period of 1 to 8 days, viability was evaluated either by measuring the fluorescence of cells labelled with viability and death fluorophores (CTG and PI respectively) through confocal microscopy or by dissociating MDTs into single cells for FACS analysis of apoptosis (Fig. 4).

Comparing MDTs to a larger format of tissue samples (LTFs), our results obtained by FACS demonstrate that MDTs maintain significantly higher viability over several days (Fig. 4B). Considering that LTFs and MDTs were cultured in similar volumetric medium to tissue ratios, this supports our hypothesis that sectioning tissue to dimensions below the critical diameter for adequate tissue oxygenation, as defined in the theory section, is important to maintain high tissue

survival under untreated conditions. We performed some preliminary cell proliferation experiments by flow cytometry (data not shown) indicating that there is cell proliferation *ex vivo* on chip over a period of 8 days, which might explain the viability recovery trend observed in Fig. 4B.

Based on our confocal microscopy results, the xenograft MDTs remain highly viable throughout the experimental period, with average viabilities above 60% for all types of xenografts. Some types of MDTs show a trend of increasing viability from day 1 to day 8. We suspect that *in vitro* cell proliferation *post* dissection might contribute to this effect. Some dead cells might also slowly shed from the tissue, leaving a higher proportion of live cells in the remaining MDT.

Given certain limitations of confocal microscopy with MDTs, in particular the imaging depth limited to about 50  $\mu\text{m}$ , the survival of the tumor tissue samples was also studied using flow cytometry after labelling the MDTs with annexin V and 7AAD, and dissociating them into single cells. As shown in Fig. 4C, initial viability was low for PC3 and highly variable for TOV112D, but higher viability values were regained over time. This reduced cell survival was probably due to the stress induced by the tissue sectioning steps. We speculate that certain types of xenografts might be more sensitive to mechanical stress and might take longer to recover from the

sectioning procedure. Nonetheless, for all types of xenografts, viabilities above 50% and sometimes as high as 85% were consistently measured after only 3 days of incubation and were maintained up to day 8.

Differences between the two viability analysis techniques might be explained by the fact that FACS provides a more complete representation of all the cells within MDTs, including centrally-located cells that are not detected with the employed confocal microscopy technique and cells washed out of the microsystems that are not accounted for by confocal microscopy. In addition, early apoptotic events are measured by FACS and thus the two techniques will not yield identical results and should therefore be regarded as complementary.

Overall, the MDT viability results from both confocal microscopy and flow cytometry suggest that the MDTs' integrity is preserved within the current device design, as shown by equal or increasing viability over the analysis period up to 8 days, across all types of xenografts tested. The viability of the xenograft MDTs was deemed sufficient for extended experimentation such a chemotherapeutic testing.

#### Long term survival of non-treated MDTs derived from patients

With an ultimate objective of performing personalized assays on *ex-vivo* primary tissue from patients, we produced MDTs

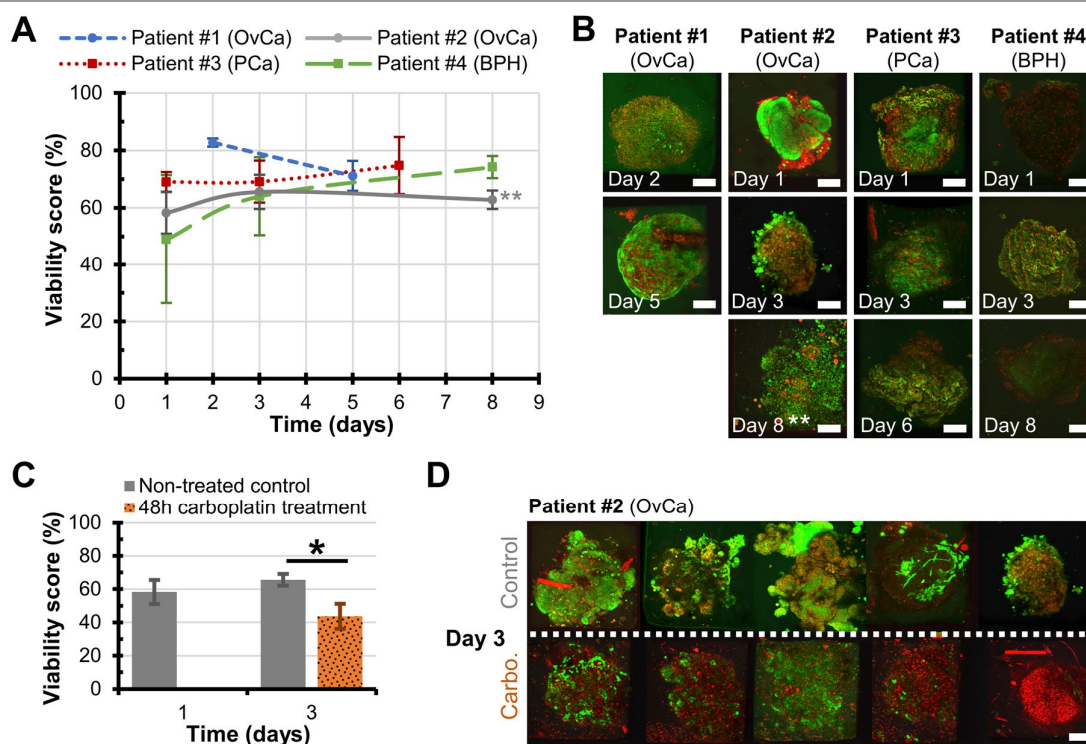


**Fig. 5:** Viability study of MDTs from four cancer patients under non-treated conditions and study of the survival of MDTs from one ovarian cancer patient after exposure to a 48-hour carboplatin treatment within the chip. **A)** Average viability score obtained by confocal microscopy for different types of non-treated patient MDTs: two ovarian cancer (OvCa) tissue samples (circle markers, blue and grey curves), one prostate cancer (PCa) tissue sample (square markers, red curve) and one benign prostatic hyperplasia (BPH) tissue sample (square markers, green curve). \*\*Result for MDTs stained and imaged a second time. **B)** Examples of confocal microscopy maximum projection images for each type of tissue (as defined in A) at different time points. Scale bar: 100  $\mu\text{m}$ . \*\*MDT stained and imaged for a second time. **C)** Average viability score obtained by confocal microscopy for non-treated MDTs and for the treated ovarian cancer MDTs from patient #2. Error bars: standard error of the mean across all MDTs exposed to a same condition. \*p-value = 0.014 for the t-test comparing results for treated MDTs to those for control MDTs. **D)** Representative confocal microscopy maximum projection images of control MDTs compared to carboplatin-treated ones. Scale bar: 100  $\mu\text{m}$ .

from patient tissue and evaluated their survival within our chip. We had access to a small portion of tissue from four different patients who had undergone surgery. Different types of patient tissue were thus obtained: two ovarian cancer tissue samples (labelled Patient #1 and #2), one prostate cancer tissue sample (Patient #3), and one non-cancer prostate tissue sample (Patient #4). Due to the small amounts of tissue available, only one type of assay was performed on these samples at two or three different time points. Confocal microscopy viability results are shown in Fig. 5A-B. A majority of live cells were detected for all types of tissues throughout the incubation period extending for up to eight days. Different tissue morphologies and staining patterns were observed in MDTs between patients, but also in MDTs from a same patient (Fig. 5B). Only a pale staining was accomplished in many of the MDTs from patient #4, which could be attributed to a slower metabolism of this benign tissue.

These tests confirm that different types of patient tissues can be sectioned into MDTs and maintained alive for several days within our microfluidic platform by following the same procedure that was optimized using mouse xenograft tissue.

#### Chemosensitivity of patient ovarian cancer MDTs to carboplatin

Some MDTs from one of the ovarian cancer patients was additionally treated with a chemotherapy. For this particular patient (patient #2 in Fig. 5), a total of 25 MDTs were loaded into a 5-channel device. Three of these channels were used as non-treated controls while the two remaining channels were treated for 48 hours (from day 1 to day 3) with carboplatin at a concentration of 350  $\mu\text{M}$ , which is equivalent to the maximum theoretical blood concentration of the drug in a normal patient treated with a 360 mg/m<sup>2</sup> dose<sup>47</sup> (see ESI for details of the calculation). At day 3, after removing the chemotherapy, significantly lower viability was detected in the treated channels compared to the controls (Fig. 5C-D). Some MDTs appeared to be less affected by the treatment (Fig. 5D, carboplatin-treated, 3<sup>rd</sup> MDT), and some regions within a single MDT also seemed to respond differently (Fig. 5D, carboplatin-treated, 1<sup>st</sup> and 2<sup>nd</sup> MDTs), which might be attributed to a variable chemoresponse of different cell subpopulations within the tumor tissue, as ovarian tumors are known to exhibit high intra-tumoral heterogeneity.<sup>48,49</sup>

As shown by using carboplatin in this experiment, the platform allows for treatments to be administered to the MDTs via microchannels, and the effects of such treatments could be assessed through confocal microscopy. These steps still need to be validated with a larger pool of patient samples and using other analysis techniques that may better capture the effects of chemotherapies.

#### Discussion

Our micro-sectioning technique produces viable submillimeter tissue sections of reproducible dimensions (Fig. 2). It has been thoroughly validated using a total of 24 xenografts formed from different types of human prostate and ovarian cancer cell

lines (Fig. 4) and four different *ex vivo* tissues from patients (Fig. 5). The technique has also been validated with four additional types of mouse xenografts (data not shown). About 300 MDTs could typically be produced from a 0.1 cm<sup>3</sup> xenograft tissue fragment and loaded into microfluidic platforms in less than six hours by a team of three people. Our approach differs from the technique developed by Jahnke *et al.*<sup>50</sup> to form tumor micro-fragments since our MDTs are immediately captured in a microfluidic device after sectioning rather than being incubated on a gyratory shaker for 48 hours and incubated in 48-well plates afterwards. In our setup, the use of a vibratome together with a biopsy punch offers better control on tissue size. MDTs can also be exposed to treatments earlier, leaving less time for undesired cell adaptation to the *in vitro* culture conditions.

With all dimensions below 500  $\mu\text{m}$ , MDTs present a number of advantages that can be exploited in cancer research. Their size range is close to the dimensions of the viable portion of cylindrical human lung tumors<sup>21</sup> and just slightly below the calculated critical diameter ( $d < 424 \mu\text{m}$ ) to avoid anoxia in spherical samples (see Theory section) such that MDTs have access to enough nutrients to remain mostly viable under untreated conditions while also mimicking natural gradients of nutrients and waste occurring in tumors (Fig. 3D-F). Their 3D structure reproduces several aspects of a tumor which are associated to reduced effectiveness of drug therapy, such as the limited delivery of drugs to their center, and varying microenvironments which may affect the metabolism and proliferation of tumor cells.<sup>51</sup> Their relatively small size also facilitates their manipulation within microsystems and eliminates the necessity to continuously perfuse the tissue. Compared to patient-derived tissue slices, a greater number of MDTs can be generated from small amounts of patient tissue. However we did note in some instances that the mechanical properties of the human tissue made them less amenable to this approach than xenografts. The micro-dissection process also consistently yielded fewer MDTs compared to xenografts of the same size, leaving room for improvement in future studies.

MDTs thus hold the potential to test multiple conditions in parallel on rare tissue biopsies, with controls in close proximity to the drug-tested regions. A sampling effect is inevitably associated to our procedure, the same way it is inherent to any technique, such as core-needle biopsies<sup>52</sup> or tumor micro-arrays (TMAs),<sup>53</sup> aiming to maximize the amount of information obtained from small volumes of tissue. This effect is nonetheless offset in our systems by the analysis of five MDTs per channel, each MDT representing a different sub-region of the initial specimen.

MDTs share several aspects with spheroids, such as a 3D structure, size, and ease of manipulation on chip. Although spheroids could be generated in larger numbers using automated methods, primary cells only rarely aggregate as spheroids, making the method an unlikely candidate for personalized medicine. Recent research has shown that spheroids could be formed from colorectal and urothelial primary cancerous tissue from patients with very high success

rates,<sup>54,55</sup> but some cellular fractions need to be discarded through the process and it remains uncertain whether the technique will be as successful for other types of tumors. By keeping the extracellular matrix intact, we expect MDTs to better preserve all cellular populations present in the original tumor, including stromal, immune, and heterogeneous subgroups of cancerous cells. Also, our technique is not dependent on the ability of cells to self-aggregate, which makes it promising for all types of solid tumors and other non-cancerous tissues.

Manipulating and tracking MDTs in a multiwell plate or in large reservoirs typically used for organotypic tissue slices would be impractical. Some microfluidic systems that were designed to capture preformed spheroids<sup>11,12</sup> could also be employed with MDTs, but we found that their resistive trapping mechanism was sensitive to perturbations provoked by normal handling of the platform, causing samples to be ejected from their traps. Trapping by sedimentation in square-bottom wells, as described here, offers superior sample stability while also shielding the samples from excessive shear stress (Fig. 3A-C) and preserving their spatial orientation for imaging purposes.

Other groups have cultured pieces or slices of primary tissue in large compartments which were continuously perfused via microfluidic channels.<sup>16,18,19</sup> Since MDTs do not need to be perfused, our systems are simpler to operate and more conditions could be tested in parallel on small amounts of tissue. An elegant approach has also been proposed by Chang *et al.*<sup>17</sup> to expose different regions of a single tissue slice to multiple conditions using only one pump. However, in their current design, tissue samples need to be imaged off-chip and their approach is not directly compatible with off-chip FACS, generally considered the gold-standard in cell analysis.

We have shown, using a high-grade serous ovarian cancer patient tissue sample, that a positive response to therapy could be measured using our approach (Fig. 5C-D). Interestingly, during clinical follow-up, the patient who received carboplatin-taxol adjuvant chemotherapy (additional to a neoadjuvant regimen prior to surgery) was identified as sensitive to treatment, so the positive response measured *in vitro* within the microfluidic chip is concordant with the clinical response of the patient.

The microfluidic platform we developed could be used in several types of assays spanning from fundamental research to clinical drug testing. The tissue within the platform could be imaged directly through the transparent PDMS bottom layer or through a modified version of the device comprising a coverslip window, which enables any microscopy technique to be employed to investigate tumor behavior. Medium fractions could also be withdrawn from the outlet of the channels to detect detached cells or components secreted by the tumors. The platform could be used not only to measure the effects of chemotherapy on patient tissue, but also to study the effects of other treatment strategies on 3D tissue in conditions that are closer to the *in vivo* setup.

## Conclusions

Our method leads to whole new possibilities for the study of patient tissue within microfluidic systems. By preserving the cell composition and organization of the original tissue while also mimicking the micro-environment of tumors, MDTs trade off some simplicity for increased biological relevance compared to the most common *in vitro* tumor models: monolayer cell cultures and spheroids. Our microfluidic platform is nonetheless operated using simple instruments typically found in any cell biology laboratory, which allows scientists to concentrate on the complex biology of the cancerous tissue and leaves place for on-chip integration of additional components. Our highly personalized technique can provide information on the drug-response profile of each patient and shows potential to improve the results of clinical trials by associating patients to the best test group, and to increase patient survival and quality of life by prescribing the most efficient treatment earlier during the course of the disease.

## Acknowledgements

This research was funded by the Québec Consortium for Drug Discovery (CQDM), Prostate Cancer Canada (PCC), the Natural Sciences and Engineering Research Council of Canada (NSERC) and the Canadian Cancer Society Research Institute (CCSRI). A.-M. Mes-Masson, F. Saad and D. Provencher are researchers of the CRCHUM, which receives support from the Fond de recherche du Québec – Santé (FRQS). M. Astolfi acknowledges graduate scholarships from NSERC and the Fonds de recherche du Québec – Nature et technologies (FRQ-NT). M. A. Lateef was supported through a grant from the Canadian Uro-Oncologist Group (CUOG). The ovarian and prostate tumor banking was supported by the “Banque de tissus et de données of the Réseau de recherche sur le cancer” of the FRQS affiliated with the Canadian Tumor Repository Network (CTRNet). We would like to thank the uro-oncologists and the gynecologic oncologists of the CHUM for providing human specimens. We also thank the staff from the animal facility, in particular Kim Leclerc Désaulniers and Maxime Thiffault, for technical support as well as Liliane Meunier, Hubert Fleury, and Dr. Philip Wong for useful discussions.

## Notes and references

- 1 M. Hay, D. W. Thomas, J. L. Craighead, C. Economides and J. Rosenthal, *Nat. Biotechnol.*, 2014, **32**, 40–51.
- 2 C. G. Begley and L. M. Ellis, *Nature*, 2012, **483**, 531–533.
- 3 E. H. Rubin and D. G. Gilliland, *Nat. Rev. Clin. Oncol.*, 2012, **9**, 215–222.
- 4 L. G. Griffith and M. A. Swartz, *Nat. Rev. Mol. Cell Biol.*, 2006, **7**, 211–224.
- 5 F. Pampaloni, E. G. Reynaud and E. H. K. Stelzer, *Nat. Rev. Mol. Cell Biol.*, 2007, **8**, 839–45.
- 6 S. Vaughan, J. I. Coward, R. C. Bast, A. Berchuck, J. S. Berek, J. D. Brenton, G. Coukos, C. C. Crum, R. Drapkin, D. Etemadmoghadam, M. Friedlander, H. Gabra, S. B. Kaye, C. J.

- Lord, E. Lengyel, D. A. Levine, I. A. McNeish, U. Menon, G. B. Mills, K. P. Nephew, A. M. Oza, A. K. Sood, E. A. Stronach, H. Walczak, D. D. Bowtell and F. R. Balkwill, *Nat. Rev. Cancer*, 2011, **11**, 719–25.
- 7 M. Zietarska, C. M. Maugard, A. Filali-Mouhim, M. Alam-Fahmy, P. N. Tonin, D. M. Provencher and A.-M. Mes-Masson, *Mol. Carcinog.*, 2007, **46**, 872–885.
- 8 J. Friedrich, C. Seidel, R. Ebner and L. A. Kunz-Schughart, *Nat. Protoc.*, 2009, **4**, 309–324.
- 9 A. Y. Hsiao, Y. S. Torisawa, Y. C. Tung, S. Sud, R. S. Taichman, K. J. Pienta and S. Takayama, *Biomaterials*, 2009, **30**, 3020–3027.
- 10 L. Y. Wu, D. Di Carlo and L. P. Lee, *Biomed. Microdevices*, 2008, **10**, 197–202.
- 11 T. Das, L. Meunier, L. Barbe, D. Provencher, O. Guenat, T. Gervais and A.-M. Mes-Masson, *Biomicrofluidics*, 2013, **7**, 011805–1 to 011805–15.
- 12 J. Ruppen, L. Cortes-Dericks, E. Marconi, G. Karoubi, R. A. Schmid, R. Peng, T. M. Marti and O. T. Guenat, *Lab Chip*, 2014, **14**, 1198–205.
- 13 B. Patra, Y. H. Chen, C. C. Peng, S. C. Lin, C. H. Lee and Y. C. Tung, *Biomicrofluidics*, 2013, **7**, 054114.
- 14 V. Vaira, G. Fedele, S. Pyne, E. Fasoli, G. Zadra, D. Bailey, E. Snyder, A. Favarsani, G. Coggi, R. Flavin, S. Bosari and M. Loda, *Proc. Natl. Acad. Sci. U. S. A.*, 2010, **107**, 8352–8356.
- 15 I. A. M. de Graaf, P. Olinga, M. H. de Jager, M. T. Merema, R. de Kanter, E. G. van de Kerckhof and G. M. M. Groothuis, *Nat. Protoc.*, 2010, **5**, 1540–1551.
- 16 P. M. Van Midwoud, G. M. M. Groothuis, M. T. Merema and E. Verpoorte, *Biotechnol. Bioeng.*, 2010, **105**, 184–194.
- 17 T. C. Chang, A. M. Mikheev, W. Huynh, R. J. Monnat, R. C. Rostomily and A. Folch, *Lab Chip*, 2014, **14**, 4540–4551.
- 18 S. M. Hattersley, C. E. Dyer, J. Greenman and S. J. Haswell, *Lab Chip*, 2008, **8**, 1842–6.
- 19 L.-T. Cheah, Y.-H. Dou, A.-M. L. Seymour, C. E. Dyer, S. J. Haswell, J. D. Wadhawan and J. Greenman, *Lab Chip*, 2010, **10**, 2720–2726.
- 20 T. Anada, J. Fukuda, Y. Sai and O. Suzuki, *Biomaterials*, 2012, **33**, 8430–41.
- 21 R. Thomlinson and L. Gray, *Br. J. Cancer*, 1955, **9**, 539–549.
- 22 I. F. Tannock, *Br. J. Radiol.*, 1972, **45**, 512–524.
- 23 W. Mueller-Klieser, *Biophys. J.*, 1984, **46**, 343–348.
- 24 K. Groebe and W. Mueller-Klieser, *Int. J. Radiat. Oncol. Biol. Phys.*, 1996, **34**, 395–401.
- 25 Y. Jiang, J. Pjesivac-Grbovic, C. Cantrell and J. P. Freyer, *Biophys. J.*, 2005, **89**, 3884–3894.
- 26 D. R. Grimes, C. Kelly, K. Bloch and M. Partridge, *J. R. Soc. Interface*, 2014, **11**, 20131124.
- 27 R. Ivanova and G. Simeonov, *Comput. Math. with Appl.*, 2012, **64**, 322–336.
- 28 P. Vaupel, H. P. Fortmeyer, S. Runkel and F. Kallinowski, *Cancer Res.*, 1987, **47**, 3496–3503.
- 29 R. Sander, *Atmos. Chem. Phys. Discuss.*, 2014, **14**, 29615–30521.
- 30 J. J. Casciari, S. V. Sotirchos and R. M. Sutherland, *J. Cell. Physiol.*, 1992, **151**, 386–394.
- 31 C. J. Koch and J. E. Biaglow, *Br. J. Cancer. Suppl.*, 1978, **3**, 163–167.
- 32 J. P. Freyer and R. M. Sutherland, *J. Cell. Physiol.*, 1985, **124**, 516–524.
- 33 A. Bertuzzi, A. Fasano, A. Gandolfi and C. Sinisgalli, *J. Theor. Biol.*, 2010, **262**, 142–150.
- 34 R. Venkatasubramanian, M. A. Henson and N. S. Forbes, *J. Theor. Biol.*, 2008, **253**, 98–117.
- 35 W. Mueller-Klieser, J. P. Freyer and R. M. Sutherland, *Br. J. Cancer*, 1986, **53**, 345–353.
- 36 J. Grote, R. Süsskind and P. Vaupel, *Pflügers Arch. Eur. J. Physiol.*, 1977, **372**, 37–42.
- 37 P. Han and D. M. Bartels, *J. Phys. Chem.*, 1996, **100**, 5597–5602.
- 38 D. M. Provencher, H. Lounis, L. Champoux, M. Tétrault, E. N. Manderson, J. C. Wang, P. Eydoux, R. Savoie, P. N. Tonin and A. M. Mes-Masson, *In Vitro Cell. Dev. Biol. Anim.*, 2000, **36**, 357–361.
- 39 M. Amiji and K. Park, *Biomaterials*, 1992, **13**, 682–692.
- 40 H. Lamb, *Hydrodynamics*, Cambridge University Press, 6th ed., 1994.
- 41 A. W. Francis, *J. Appl. Phys.*, 1933, **4**, 403–406.
- 42 W. L. Haberman and R. M. Sayre, *Motion of fluid spheres in stationary and moving liquids inside cylindrical tubes*, 1958.
- 43 J. Markiewicz and W. R. Matson, *Am. J. Mod. Phys.*, 2013, **2**, 98.
- 44 M. Khabiry, B. G. Chung, M. J. Hancock, H. C. Soundararajan, Y. Du, D. Cropek, W. G. Lee and A. U. Khademhosseini, *Small*, 2009, **5**, 1186–1194.
- 45 R. Venkatasubramanian, M. A. Henson and N. S. Forbes, *J. Theor. Biol.*, 2006, **242**, 440–453.
- 46 J. P. Ward and J. R. King, *IMA J. Math. Appl. Med. Biol.*, 1997, **14**, 39–69.
- 47 R. R. Barakat, A. Berchuck, M. Markman and M. E. Randall, *Principles and Practice of Gynecologic Oncology*, Wolters Kluwer, 6th ed., 2013.
- 48 L. Khalique, A. Ayhan, M. Weale, I. Jacobs, S. Ramus and S. Gayther, *J. Pathol.*, 2007, **211**, 286–295.
- 49 S. L. Cooke, C. K. Y. Ng, N. Melnyk, M. J. Garcia, T. Hardcastle, J. Temple, S. Langdon, D. Huntsman and J. D. Brenton, *Oncogene*, 2010, **29**, 4905–4913.
- 50 H.-G. Jahnke, S. Poenick, J. Maschke, M. Kendler, J. C. Simon and A. A. Robitzki, *Cancer Res.*, 2014, **74**, 6408–6418.
- 51 O. Trédan, C. M. Galmarini, K. Patel and I. F. Tannock, *J. Natl. Cancer Inst.*, 2007, **99**, 1441–1454.
- 52 C. Öbek, T. Doanca, S. Erdal, S. Erdoğan and H. Durak, *J. Urol.*, 2012, **187**, 2051–2055.
- 53 M. Ilyas, H. Grabsch, I. O. Ellis, C. Womack, R. Brown, D. Berney, D. Fennell, M. Salto-Tellez, M. Jenkins, G. Landberg, R. Byers, D. Treanor, D. Harrison, A. R. Green, G. Ball and P. Hamilton, *Histopathology*, 2013, **62**, 827–839.
- 54 J. Kondo, H. Endo, H. Okuyama, O. Ishikawa, H. Iishi, M. Tsujii, M. Ohue and M. Inoue, *Proc. Natl. Acad. Sci. U. S. A.*, 2011, **108**, 6235–40.
- 55 H. Okuyama, T. Yoshida, H. Endo, M. Nakayama, N. Nonomura, K. Nishimura and M. Inoue, *J. Urol.*, 2013, **190**, 302–310.